

A Sensitized Plastic Fiber Sensor for Multi-Point Bending Measurement Based on Deep Learning

Shun Lu , Zhongwei Tan, Guangde Li, and Jingya Yang

Abstract—As we all know, the change of mode interference caused by the curvature change in multi-mode fiber (MMF) can be well represented as a fiber specklegram recorded by CCD (Charge-coupled Device). However, it's difficult to identify the different bending occurred in several points in short distance. The paper proposes plastic fiber bending sensors can be used to detect the multi-point bending without adding any hardware. The convolutional neural network was used to classify the output speckles under different bending states. Specklegrams from fiber with three sensitization areas can be recognized by the neural network with a bending interval of 15° , 10° and 5° with an accuracy rate of 99.2%, 96.1% and 93.5% respectively. Compared with traditional multi-point distributed sensors, this method is lower cost and easier to operate. The method proposed in this paper can find applications in distinguishing the status of certain structures, such as robotic arms and some disabled auxiliary equipment.

Index Terms—Multi-point bending sensor, sensitized plastic fiber, fiber specklegram, deep learning, convolutional neural network.

I. INTRODUCTION

SINCE optical fiber technology has brought epoch-making changes to the field of communication, it has also greatly promoted the development of sensing field. Optical fiber sensing is an emerging technology, that utilizes the characteristics of waveguide fiber to transform the changes of external measured physical quantities into the changes of some characteristic parameters, such as amplitude, phase, polarization state, frequency and wavelength to realize the purpose of sensing [1]. Fiber sensors have played a crucial role in many applications, including bridge security monitoring [2], biochemical sensing [3], gas detectors [4] and power system monitoring [5]. Plastic optical fibers (POF) were first proposed in the 1960s and had grown slowly over the years until Professor Koike of Keio University invented the graded index plastic fiber and obtained the low-loss fluorinated plastic fiber in 1990. Plastic optical fibers have the inherent advantages of quartz fiber and are flexible and easy to handle [6]. Plastic optical fibers, a kind of multimode fiber,

can adapt to more complex environments due to their high malleability. Lee Danisch invented a fiber optic curvature sensor using a fiber with the cladding and part of the fiber core surface was destroyed [7]. When the fiber is bent, more light will leak from the fiber, and the light intensity at the output end will decay exponentially with the increase in curvature, so that the sensitivity of the sensor is improved. A bending sensor based on light intensity is used to measure finger bending [8]. However, a drawback of light intensity variation-based sensors is the lack of multiplexing capabilities.

In recent years, multi-point bending sensors using multicore fiber and Bragg grating have also been proposed. Some scholars have used the characteristics of the multicore fiber and the change of the reflectional wavelength of Bragg grating to measure the different bending states of fiber. [9]–[10]. A research team has also achieved distributed bending sensing by measuring the Brillouin frequency shift in the outer core of a multi-core fiber. They used a seven-core fiber, with one core placed at the optical fiber's geometric center and six other cores evenly distributed around it. When the multi-core fiber is bent, the strain generated by the outer core is much larger than that of the middle core, so the bending measurement can be realized by measuring the Brillouin frequency shift of the outer core [11]–[12]. Complex measurement systems and complicated operation principles have hindered their portability and applications to multi-point bending measurement.

Some scholars have proposed a great method to use different colors of light to solve the problem of multiplexing capabilities to achieve multi-point sensors [13]. But the sensor can only discriminate a few points' bending limited by colors and it can't achieve high sensitivity because of the limit of the sensitivity of light intensity. Our method is not color sensitive and can be used together with the multi-color multiplexing method to enlarge the number of sensors and enhance its accuracy. Due to the change of environmental factors, many transmission modes in multimode fiber may cause internal mode coupling and dispersion. If the light is coupled to the input of multi-mode fiber, a kind of specklegram that cannot be recognized by human eyes will be obtained at the output end [14]. A speckle pattern can be created by the propagated modes interfering within the optical fiber. Each point of the field distribution (speckle) combines of several contributions with aleatory phases and depends on the fiber stability [15]. Thus, the speckle pattern is sensitive to changes on their propagating medium and can be employed as sensing elements. Due to the bending of multimode fiber will cause the coupling of fiber transmission modes, different coupling

Manuscript received June 11, 2021; revised July 21, 2021; accepted August 3, 2021. Date of publication August 10, 2021; date of current version September 15, 2021. This work was supported by the National Science Foundation of China under Grants 61875008 and 61975009, and in part by Goolton Technology Company, Ltd. (Corresponding author: Zhongwei Tan.)

The authors are with the Key Lab of All Optical Network & Advanced Telecommunication Network Ministry of Education, Institute of Lightwave Technology, Beijing Jiaotong University, Beijing 100044, China (e-mail: shunlu@bjtu.edu.cn; zhwtan@bjtu.edu.cn; 18120006@bjtu.edu.cn; 18120159@bjtu.edu.cn).

Digital Object Identifier 10.1109/JPHOT.2021.3103566

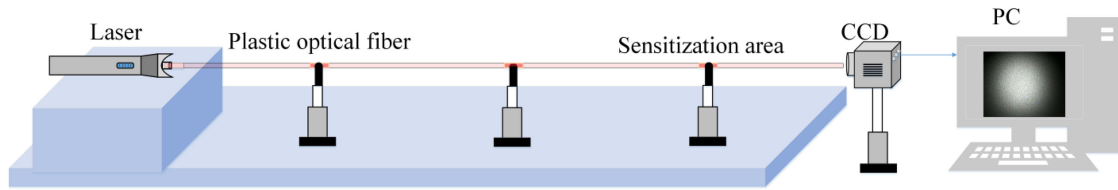


Fig. 1 Experimental structure diagram.

modes will lead to different mode field distribution at the output and different speckle patterns will be generated. Therefore, the multi-point bending sensor can be constructed by establishing the relationship between the various speckles and the multi-state bending of the optical fiber. There are millions of transmission modes in plastic fiber, thus it is difficult to distinguish speckles produced by different modes.

With the development of machine learning, many deep learning algorithms have been applied to the recognition of complex images. In recent years, deep learning is widely used in the identification and reconstruction of speckle output by multimode fiber [16]–[18]. Last year, a fiber bending curvature sensor based on deep learning was proposed [19]. This sensor uses single mode-multimode-single mode (SMS) fiber structures as the transmission medium. However, this kind of sensor measures the bending curvature of the entire optical fiber, neither aiming at a certain point on the optical fiber, nor can it achieve the measurement of multi-point bending of the optical fiber.

Based on the relevant studies, a new category of multi-point bending sensor based on deep learning is proposed in this paper. Because plastic optical fiber is easier to be polished and sculpted, we handle plastic fiber to construct this sensitized fiber bending sensor. It has been proved that deep learning can discriminate the different images at the fiber end [16]–[19]. Different bending sensitive areas of the sensitized fiber will cause mode changes, which can be seen as transmitting different images to the end of the fiber, so different bending can be classified to make a multi-point bend sensor. A deep learning algorithm is used to identify the output speckle of the bending fiber and analyze the bending angles in different sensing areas. In the experiment, a plastic optical fiber with sensitized areas was used to test the performance of the sensor. We collected the speckles of the fiber output when the sensitized areas were bent independently and simultaneously, and the collected speckle patterns are classified by Convolutional Neural Network (CNN) [20], which is used to complete the detection of different bending angles and bending areas of the fiber. As a contrast, we also use the SVM algorithm to classify speckles. This method does not require a complex detection system. Due to the large amounts of speckle are used for training, it can overcome the sensing error caused by noises, which has great potential in the field of fiber bending detection [21].

II. EXPERIMENTAL STRUCTURE AND FABRICATION OF SENSITIZED FIBER SENSOR

An experimental setup to detect speckle pattern is shown in Fig. 1. Plastic fiber is placed on a stable experimental platform.

Each sensitized area is regulated by clamp, and the bending angle of each point can be changed by moving the clamp. The position of the fiber input will move according to the change in the bending state of the fiber. The laser is connected to the fiber input, so it can be moved according to the position of the fiber input. CCD is fixed and set at the output of the fiber to capture speckle. In this experiment, the continuous light output from the fiber output was recorded as video by CCD, whose frame rate is 30 frames per second. All the recorded videos were stored on a hard drive until the dataset complete. After that, each video converted into specklegram with 340×340 resolution.

In the experiment, two different kinds of optical fibers are used for testing. The structure of the two kinds of optical fibers is shown in the Fig. 2(d) and Fig. 2(e), in which the Fig. 2(d) shows the fiber with three sensitization area and Fig. 2(e) shows fiber with two sensitization area. The yellow part of the fiber is the sensitive area of bending, and the orange part of the fiber is the sensitive area in the unbent state. The total length of two fibers is 60cm. The sensitized areas on the plastic optical fiber are located on 15cm, 30cm and 45cm away from input end of the fiber with three sensitized areas. The sensitized areas on the plastic optical fiber are located on 20cm and 40cm away from input end of the fiber with two sensitization areas.

As we all know, optical fiber's surface can be disposed to make the sensor have greater sensitivity [22]–[23]. Its structure diagram is shown in Fig. 2(a) [24]. To increase the fiber's sensitivity to bending deformation, a part of the fiber core is removed and the remaining light after the loss still propagates along the fiber. As shown in Fig. 2(b), the direction that bends in the opposite direction to the sensitive areas is called forward bending. In the forward bending, more light will leak from the sensitized area, resulting in the change of output light intensity and transmission mode. The angle of incident light is θ and the bending radius of the optical fiber is R . Fig. 2(c) shows the manufacturing method of the sensitized optical fiber in this experiment. Firstly, the plastic optical fiber is fixed in the mold, and then the top of the plastic fiber is polished with a file. The width of grinding is 1cm.

In terms of optical fiber transmission mode variation, due to there are many modes in plastic fiber, it is difficult to use a unified formula to express the loss caused by bending. Mode coupling occurs between the high order mode and the low order mode in the fiber when axial bending occurs, so that the power in the fiber is redistributed among the modes. With the changing of the bending curvature, the conducting mode in the fiber core will radiate after passing through the sensitization area, resulting in a radiated mode that leaks out of the fiber. After the light passes through the sensitization area, it will re-couple in the fiber to

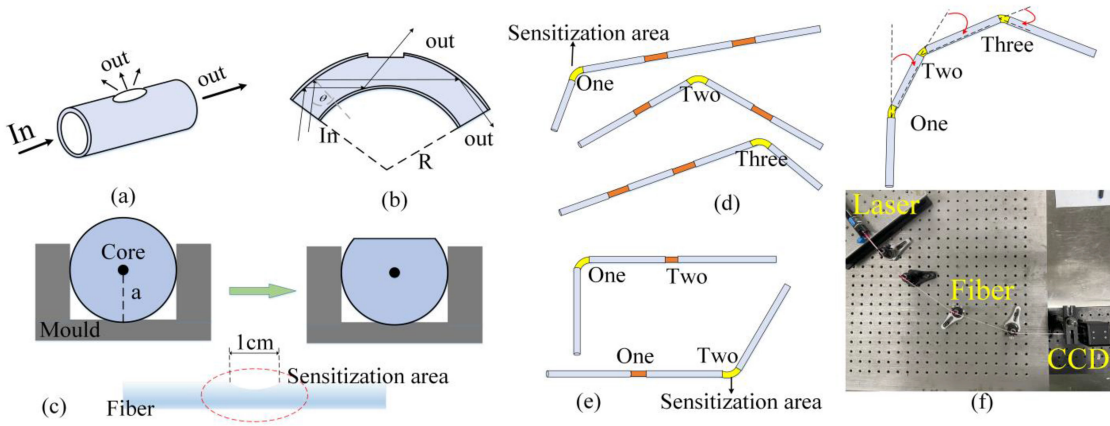


Fig. 2. (a) Structure diagram of sensitized fiber. (b) Forward bending of the fiber. (c) Fabrication of sensitized plastic optical fiber. (d) Structure of fiber with three sensitized areas. (e) Structure of fiber with two sensitized areas. (f) Structure of three sensitized areas are bent simultaneously.

generate a new mode, so that the mode change at the end of the sensitized fiber will be larger [25].

When the light passes through the sensitized fiber, the intensity of the light changes as the fiber bending, it can be denoted by Eq. (1)

$$p = \eta p_0 \exp \left\{ -\frac{1}{4} \frac{zK^2}{a} \left[1 - \left(\frac{R-a}{R+a} \sin \theta \right)^2 \right]^{1.5} \times \left(\frac{R-a}{R+a} \sin \theta \right) \right\} \quad (1)$$

Where P and P_0 are output and input of light intensity, respectively. η is the proportional coefficient of optical power loss. Then, R and a are respectively the bending radius and fiber radius of the fiber. K denotes characteristic index of the sensitized area, θ is the angle of the angle of incidence, z is the transmission distance. Obviously, the above parameters have impacts on the intensity of output light. In the experiment, we just take R as the variable and other values remain unchanged.

The change of fiber transmission mode and the change of light intensity can both affect the speckle change of fiber output together. The change of light intensity can affect the brightness of the whole speckle and the change of transmission mode will affect the value of each pixel on the speckle. In this paper, the fiber is bent in the opposite direction of the cut, which during the fiber bending process will cause part of the light leakage. Obviously, it will increase the change of the transmission mode and the change of output light intensity, and make the collected speckle pattern variation larger to achieve better classify effect.

III. METHOD AND EXPERIMENT

In the experiment, the sensitive area bends in turn and we have collected the speckle output of the fiber when the bending step is 5° . When one sensitized area is bent, others sensitized areas remain unbent, the speckle patterns with forward bending ranging from 0° to 90° with a spacing of 5° are successfully collected by the remote CCD for each sensitized area. 340 pictures are saved for each Angle, and a total of 18700 speckle

patterns were collected. In order to explore the performance of this bending sensor, we take the speckles with bending steps of 15° , 10° and 5° as three comparative experiments. From 0° starts to 90° , When the bending step is 15° , the speckle patterns of 0° , 15° , 30° , 45° , 60° , 75° and 90° is used for experiment. In addition of the speckle collected without fiber bending, a total of 18 different categories of speckle patterns are collected for fiber with three sensitized area, and these 19 different categories of speckles are labeled with numbers from 0-18. The 6460 speckle patterns are divided into 3 groups as training set, test set, and verification set. The training set consists of 4560 speckle patterns, the test set contains 760 speckle patterns and verification set is composed of 1140 speckle patterns. Similarly, we selected speckles with bending steps of 10° , and speckles with bending steps of 5° for experiment, the datasets of two experiments had 28 and 55 speckle categories, respectively. We have also carried out another experiment with fiber of two sensitized area. The operation procedure is as same as the three-point bending experiment and the bending step is 15° . Due to the lack of a bending point, only 13 different categories of speckle patterns have been collected in the experiment, and these 13 different categories of speckles are labeled with numbers from 0-12. Each category with 340 speckles is captured by CCD. 4420 speckle patterns have been collected for training, validation and testing, in which the training set consists of 3120 speckle patterns and the test set contains 520 speckle patterns and verification set is composed of 780 speckles. In addition to single point bending, we also tested the performance of this bending sensor when all the three areas are bent simultaneously, the fiber structure and experimental structure are shown in Fig. 2(f), the yellow part of the fiber is the sensitive area of bending. The bending angles of the three areas can be 15° , 30° and 45° , each different combination of angles represents a new category of speckle that can be collect, a total of $3 \times 3 \times 3 = 27$ different categories of speckles collected. Furthermore 340 speckles of each category as well were collected, in which 6480 speckle patterns are used for train, then 1620 speckle patterns are used for verification, to finalize 1080 speckle patterns are used for test.

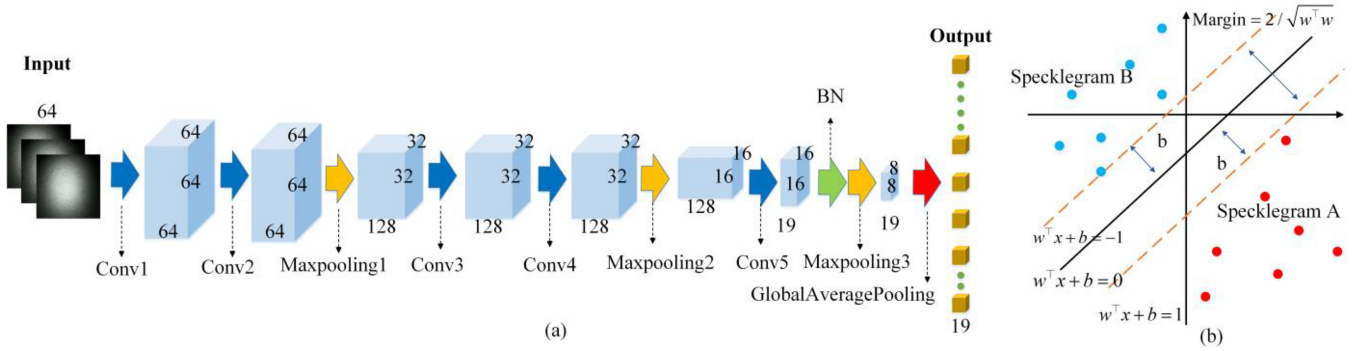


Fig. 3. (a) Convolutional neural network. (b) SVM algorithm structure diagram.

It should be noted that the stability of the whole experiment system should be guaranteed during the experiment. Because the instability of the system will cause the fluctuation of the specklegrams, which will affect the accuracy of speckle recognition.

Convolutional Neural Network (CNN) has been widely used in the field of image recognition and target classification. Because it needs a large amount of data sets for training and learning, the method can overcome the interference of disadvantaged data and reduce the experimental error. In this paper, we adopt the standard block-structure of Alex-Nets as our algorithm structure, which is an excellent algorithm mode proposed in 2014. According to the size of the training set, a neural network composed of 5 convolutional layers is designed, which can be seen in Fig. 3 for details. The neural network is mainly composed of convolution layer, pooling layer and global average pooling layer. The blue arrow represents convolution operation, the yellow one represents pooling operation, the green one represents Batch Normalization and the red one represents Global Average Pooling. The speckle collected by the experiment is resize to 64×64 before sent to the neural network. Since the first convolution uses 64 convolution kernels of 3×3 size for convolution, the parameter of feature map obtained after the convolution is $64 \times 64 \times 64$. Among them, 64×64 is the size of each image after the convolution, and the last '64' is the number of feature images after the convolution. Before the convolution of each image, the padding operation should be completed to ensure that the size of the image after the convolution remains unchanged. Activation function should be added after each convolution operation to avoid gradient explosion and gradient vanishing problems. The activation function used in this network is RELU function, which is define as $RELU = \max(0, x)$. The convolutional layers within each block take the convolution of the stack of input feature map X_k^q using weights W_k^q . Mathematically, the convolution operator outputs the input feature maps as Eq.2.

$$X_{k+1}^q(i, j) = \sum_a \sum_b X_k^q(i + a, j + b) W_k^q(a, b) \quad (2)$$

Where i and j denote the pixels in the feature map, W_k^q indicates a kernel of weights belonging to the k -th layer and the q -th convolution, a and b denote the pixel indices of

the kernels. The second convolution is the same operation as the first. Then the convoluted feature map is input into the pooling layer for feature extraction, and the size of the feature map becomes 32×32 after 2×2 pooling (Maxpooling1). Conv3 and Conv4 have 128 convolution kernels in which kernel size is 3×3 . Similarly, after the convolution of Conv3, Conv4 and 2×2 pooling operation of Maxpooling2, the size of the feature map becomes 16×16 , and the number of the feature map becomes 128. The characteristic map outputted by Conv4 is then input to Conv5. Conv5 have 19 kernels, which correspond to the number of output channels and depend on the number of input categories. Batch Normalization (BN) has the characteristic of improving network generalization ability. After passing through BN and Maxpooling3, feature map whose size is $8 \times 8 \times 19$ is obtained from the output of Conv5. Global Average Pooling can pool the feature map of the last layer by one mean value of the whole picture to form a feature point, which can be used to form the final feature vector for calculation in SoftMax. Compared with the traditional full connection layer, after extracting the feature image of Convolutional Neural Network, Global Average Pooling can reduce computational parameters to avoid overfitting and improve the performance of the network. It is worth mentioning that a deeper neural network will improve the nonlinear fitting ability of the network and can adapt to more complex recognition tasks, but it will also increase the training time of network. Therefore, the number of network layers is empirically chosen based on a trade-off among the network's complexity. The CNN is implemented using the TensorFlow 1.6 Python library on a single NVIDIA GeForce GTX 1050Ti graphics processing unit, Adam Optimizer with a learning rate of 0.0001 is used to updating the network parameters.

In order to verify the superiority and reliability of the algorithm, we also used the SVM (Support Vector Machines) algorithm to classify speckles under different bending conditions. The basic idea of SVM is to obtain a separating hyperplane that can correctly divide the training data set and have the maximum geometric interval. Taking image classification as an example, the number of pixels of an image is understood as the number of dimensions, then each picture is represented by the point in this high-dimensional space. But high-dimensionality cannot be visualized. Therefore, we use a two-dimensional graph as an analogy to illustrate the role of linear classifiers. As

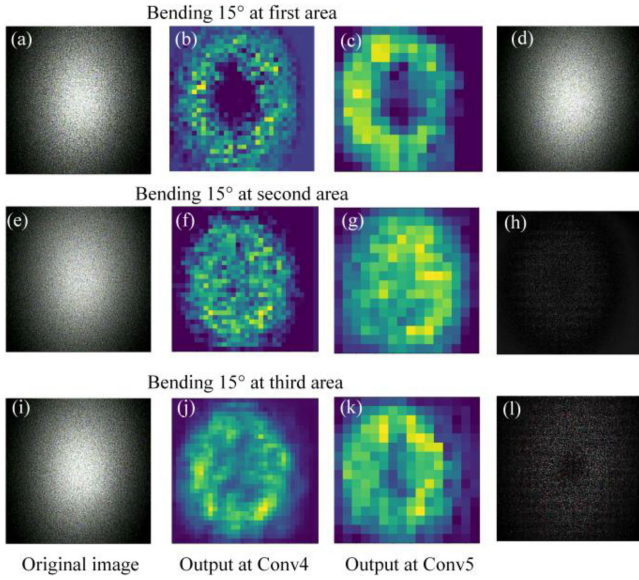


Fig. 4. Visualization of specklegrams and CNN extracted feature maps.

shown in Fig. 3(b), $w^T x + b = 0$ is the separated hyperplane, there are infinitely hyperplanes for linearly separable data set, but the separating hyperplane with the largest geometric interval is unique. The data set in this two-dimensional space is $T = \{(x_1, y_1), (x_2, y_2), \dots, (x_n, y_n)\}$, where $x_i \in \mathbb{R}^n$, and $y_i \in \{+1, -1\}$, $i = 1, 2, \dots, N$, x_i denote the number i of the specklegram. Assume that y is equal to 1 and -1 represents Specklegram A and Specklegram B respectively. The mathematical of restricted conditions is denoted by $w^T x + b \geq +1, y_i = 1, w^T x + b \leq -1, y_i = -1$. Margin can be denoted as $2/\sqrt{w^T w}$. Therefore, the problem of solving the SVM model can be expressed as a problem of finding maximum of the Margin under restricted conditions. In this experiment, the SVM is implemented using the SVM function in the ‘scikit-learn’ library in Anaconda.

IV. ANALYSIS AND DISCUSSION

The speckle patterns collected with CCD and feature map extracted by CNN are shown in Fig. 4. Due to the data sets are large, only three types of speckles are listed in this paper for example. Fig. 4(a), Fig. 4(e) and Fig. 4(i) denote the collected specklegrams of the three sensitized areas by bending 15° , respectively. Fig. 4(b), Fig. 4(f) and Fig. 4(j) show the feature maps collected in Conv4. Fig. 4(c), Fig. 4(g) and Fig. 4(k) show the feature maps collected in Conv5. It can be found that speckle will become an abstract feature images after multiple convolutions, which can help Global Average Pooling to have a better classification. Fig. 4(a) and Fig. 4(d) are two speckles collected within three seconds under the same bending state, and picture shown in Fig. 4(h) is the difference caused by noise fluctuations between two speckles, Fig. 4(l) is the difference between Fig. 4(a) and Fig. 4(i), it can be found that transform of the speckle caused by different bends is more obvious than the

transform of speckle caused by noise. Since the light transmission in the fiber is an unstable transmission system, we cannot avoid the influence of these factors on the experiment. However, according to the results identified by CNN, it is found that the deep learning algorithm can reduce the influence of these factors on the final experimental results.

As shown in Fig. 5, During the learning process, the training history and classification performance of the Convolutional Neural Network trained with the specklegrams, are plotted as a function of the iteration number. The loss function is used to measure the performance of the model and inconsistency between actual value and predicted value. After each Epoch operation is completed, a loss which is used to update the weight in the network will be calculate. The loss function is defined as follows:

$$loss = - \sum_{i=1}^n y_{i1} \cdot \log \hat{y}_{i1} + y_{i2} \cdot \log \hat{y}_{i2} + \dots + y_{im} \cdot \log \hat{y}_{im} \quad (3)$$

In Eq. (3), n represents the number of specks during training, m refers to the number of categories in this experiment, y and \hat{y} are the label of the input speckle and the predicted value of the network’s output to speckle, respectively. The accuracy is defined as the ratio between the correct classifications and total classifications. Fig. 5(a) and Fig. 5(b), when the bending step is 15° , respectively represents the training process of speckle, which collected by two different fibers. It can be seen from Fig. 5(a) and Fig. 5(b) that the accuracy rate of the training set increases steadily and reaches over 99.6% and 98.5%. According to Fig. 5(c), specklegrams which captured with fiber is bent simultaneously with different combination of angles can also be well classified, and the training accuracy rate reached 95%. Although the accuracy rate of the verification set fluctuates are not much, the overall upward trend is consistent with the training set. There is no upward trend during the training of training set and verification set. Therefore, during the training, it can be concluded that there is no overfitting phenomenon occurs. In the initial stage of training, the accuracy and loss curves of the verification set cannot fit well with the curves of the training set, it might be cause of the fluctuation, which speckle caused by the noise in the external environment. However, it is found that this situation didn’t affect the recognition accuracy of the test set.

In the experiment, 520 specklegrams are used as the test set for the fiber with two sensitized areas. The 13 sets of data mentioned above are labeled with 13 different labels. The confusion matrix of the test results is shown in Fig. 6(a), where the horizontal axis represents the true label of the specklegrams, the vertical axis represents the label predicted by the neural network for the specklegrams, and the numbers in the figure represent the predicted probabilities of different categories of speckles. The 760 specklegrams which bending step of 15° are divided into 19 groups and used as the test set for fiber with three sensitization area. The confusion matrix of test results is shown in Fig. 6(b). According to the results of test set, the accuracy of predicting is 99.6% and 99.2% for fiber with two sensitization area and fiber with three sensitization area. Compared with the former,

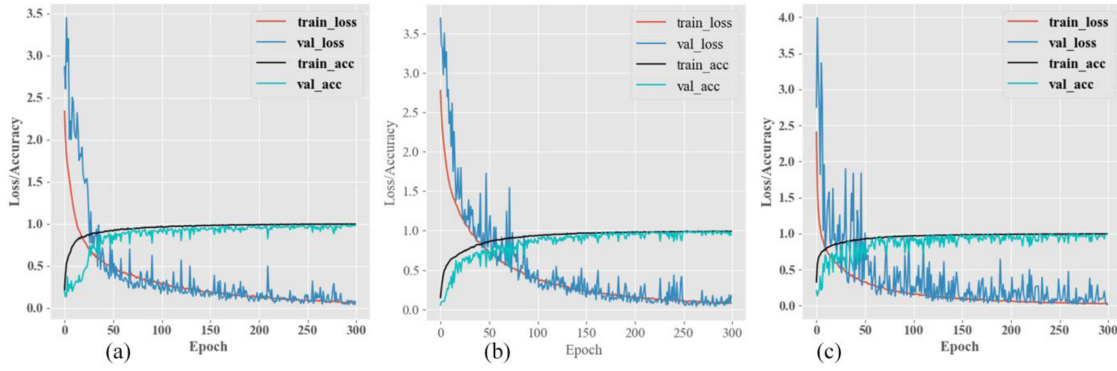


Fig. 5. Network model training process based on specklegrams from (a) fiber with two sensitive area, (b) fiber with three sensitive area and (c) Three areas bent simultaneously.

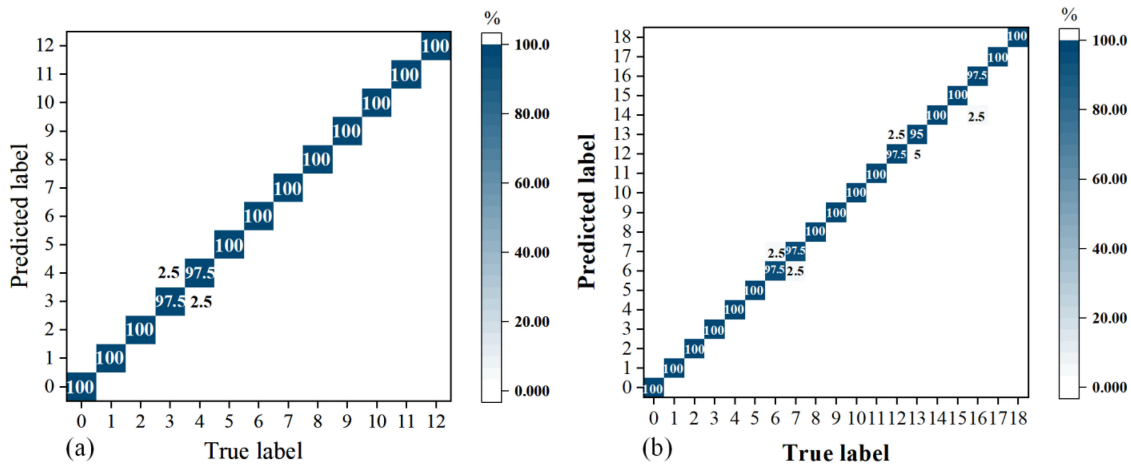


Fig. 6. Network model training process based on specklegrams from (a) fiber with two sensitive area and (b) fiber with three sensitive area.

TABLE I
RESULTS OF THE TEST ACCURACY WHEN USING DIFFERENT FIBERS AND DIFFERENT ALGORITHMS

Bending state	Fiber	Number of types	The accuracy of SVM	The accuracy of CNN
The area is bent with bending step is 15°	The fiber with two sensitized area	13	98.4%	99.6%
The area is bent with bending step is 15°	The fiber with three sensitized area	19	98.8%	99.2%
The area is bent with bending step is 10°	The fiber with three sensitized area	28	95.9%	96.1%
The area is bent with bending step is 5°	The fiber with three sensitized area	55	94%	93.5%
Three areas bent simultaneously	The fiber with three sensitized area	27	93.2%	94%

the accuracy of the latter decreases slightly as the sensitized area increases. It shows that the use of convolutional neural networks can well classify the output speckles of plastic optical fibers under different bending degrees.

For the fiber with three sensitized areas, the bending step of 5° and 10° are also tested. As shown in Table I, when the bending step is 10° , a total of 28 categories of specks are classified, and the recognition accuracy of SVM algorithm and CNN algorithm are 95.9% and 96.1% respectively. When the bending step is 5° , the total of 55 categories of specks are classified, and the recognition accuracy of the two algorithms is 94% and 93.5%

respectively. In the case of three sensitized areas are bent simultaneously with different combination of angles, the total of 27 categories of specks are classified, and the accuracy of the two algorithms can reached 93.3% and 93.9%.

According to Table I, it can be found that the recognition accuracy of the two algorithms gradually decreases as the bending step size decreases and the number of bending categories increases.

In the experiment, the recognition accuracy of CNN algorithm and SVM algorithm proposed in this paper are similar and both achieve high accuracy, which indicates that under

different bending states, the speckle output of the sensitized fiber has high-dimensional characteristics and can be well classified. Moreover, in more cases, CNN proposed in this paper shows better classification effect.

V. CONCLUSION

In this paper, the theory of sensitized optical fiber bending sensor is analyzed and a kind of multi-point bending sensor based on convolutional neural network is proposed. The experimental results show that deep learning can distinguish where the bending occurs on the fiber and the value of the bending angle. When bending step is 15° , the detection accuracy reaches 99.6% and 99.2% for sensor with different number of sensitized areas. For the fiber with three sensitized areas, when the bending step is 10° and 5° , the classification accuracy of specklegrams reaches 96.1% and 93.5%. When three areas bent simultaneously, the classification accuracy of 27 bending combinations is 94%. The experiment confirms the feasibility and superiority of this method when all the three points are bent simultaneously. It proves that this method can be used in multi-point fiber bending sensors.

Different from the traditional bending sensor, the sensor introduced in this article has the three advantages. First, the sensor uses a sensitized optical fiber which is cheap and simple in structure to improve the sensitivity of bend sensing. Secondly, the sensor avoids measuring the spectrum can effectively reduce the cost. Finally, using the change of the speckles to indicate the change of the mode instead of measuring the change of light intensity can improve the accuracy and sensitivity of the sensor. Multi-point bending sensors have a wide range of applications in fields such as manipulators and biological monitoring. With the development of deep learning, there will be more and more excellent algorithms to achieve better classification and recognition results in the future.

In addition, the structure of sensitized fiber can be changed with fiber grating to improve the sensitivity of speckles output at end of the fiber. If this kind of technology is applied to the field of manipulators, it is necessary to consider the bending of the optical fiber in three-dimensional space, which will be future research direction for us.

REFERENCES

- [1] K. T. V. Grattan and T. Sun, "Fiber optic sensor technology: An overview," *Sens. Actuator A-Phys.*, vol. 82, no. 1-3, pp. 40–61, May 2000, doi: [10.1016/S0924-4247\(99\)00368-4](https://doi.org/10.1016/S0924-4247(99)00368-4).
- [2] R. Maaskant, T. Alavie, R. M. Measures, G. Tadros, S. H. Rizkalla, and A. GuhaThakurta, "Fiber-optic Bragg grating sensors for bridge monitoring," *Cem. Concr. Compos.*, vol. 19, no. 1, pp. 21–33, Feb. 1997, doi: [10.1016/S0958-9465\(96\)00040-6](https://doi.org/10.1016/S0958-9465(96)00040-6).
- [3] F. Baldini, M. Brenci, F. Chiavaioli, A. Giannetti, and C. Trono, "Optical fibre gratings as tools for chemical and biochemical sensing," *Anal. Bioanalytical Chem.*, vol. 402, no. 1, pp. 109–116, Jan. 2012, doi: [10.1007/s00216-011-5492-3](https://doi.org/10.1007/s00216-011-5492-3).
- [4] X. Qin, W. L. Feng, X. Z. Yang, J. W. Wei, and G. J. Huang, "Molybdenum sulfide/citric acid composite membrane-coated long period fiber grating sensor for measuring trace hydrogen sulfide gas," *Sensors Actuators B-Chem.*, vol. 272, pp. 60–68, Nov. 2018, doi: [10.1016/j.snb.2018.05.152](https://doi.org/10.1016/j.snb.2018.05.152).
- [5] H. Park, M. Song, and 김현진, "A quasi-distributed fiber-optic sensor system using an InGaAs PD array and FBG sensors for the safety monitoring of electric power systems," *J. Korean Inst. Illum. Elect. Installation Engineers*, vol. 24, no. 2, pp. 86–91, 2010, doi: [10.52077/jieie.2010.24.2.086](https://doi.org/10.52077/jieie.2010.24.2.086).
- [6] L. Bilro, N. Alberto, J. L. Pinto, and R. Nogueira, "Optical sensors based on plastic fibers," *Sensors*, vol. 12, no. 9, pp. 12184–12207, Sep. 2012, doi: [10.3390/s120912184](https://doi.org/10.3390/s120912184).
- [7] L. A. Danisch, "Fiber optic bending and positioning sensor including a light emission surface formed on a portion of a light guide," Patent No. 5,321,257, Jun. 14, 1994.
- [8] H. T. Di, Y. T. Li, K. Y. Liu, L. H. An, and J. F. Dong, "Hand gesture monitoring using fiber-optic curvature sensors," *Appl. Opt.*, vol. 58, no. 29, pp. 7935–7942, Oct. 2019, doi: [10.1364/ao.58.007935](https://doi.org/10.1364/ao.58.007935).
- [9] D. Zheng, J. Madrigal, H. L. Chen, D. Barrera, and S. Sales, "Multicore fiber-Bragg-grating-based directional curvature sensor interrogated by a broadband source with a sinusoidal spectrum," *Opt. Lett.*, vol. 42, no. 18, pp. 3710–3713, Sep. 2017, doi: [10.1364/ol.42.003710](https://doi.org/10.1364/ol.42.003710).
- [10] M. Hou *et al.*, "Two-dimensional vector bending sensor based on seven-core fiber Bragg gratings," *Opt. Exp.*, vol. 26, no. 18, pp. 23770–23781, Sep. 3, 2018, doi: [10.1364/oe.26.023770](https://doi.org/10.1364/oe.26.023770).
- [11] Z. Y. Zhao, M. A. Soto, M. Tang, and L. Thevenaz, "Distributed shape sensing using Brillouin scattering in multi-core fibers," *Opt. Exp.*, vol. 24, no. 22, pp. 25211–25223, Oct. 2016, doi: [10.1364/oe.24.025211](https://doi.org/10.1364/oe.24.025211).
- [12] M. Hou *et al.*, "Two-dimensional vector bending sensor based on seven-core fiber Bragg gratings," *Opt. Exp.*, vol. 26, no. 18, Sep. 3, 2018, Art. no. 23770, doi: [10.1364/OE.26.023770](https://doi.org/10.1364/OE.26.023770).
- [13] H. Bai, S. Li, J. Barreiros, Y. Tu, C. R. Pollock, and R. F. Shepherd, "Stretchable distributed fiber-optic sensors," *Science*, vol. 370, no. 6518, pp. 848–852, Nov. 13, 2020, doi: [10.1126/science.aba5504](https://doi.org/10.1126/science.aba5504).
- [14] N. Borhani, E. Kakkava, C. Moser, and D. Psaltis, "Learning to see through multimode fibers," *Optica*, vol. 5, no. 8, pp. 960–966, 2018, doi: [10.1364/optica.5.000960](https://doi.org/10.1364/optica.5.000960).
- [15] J. W. Goodman, *Speckle Phenomena in Optics: Theory and Applications*. Roberts and Publishers, 2007, pp. 27–37.
- [16] P. Wang and J. Di, "Deep learning-based object classification through multimode fiber via a CNN-architecture speckleNet," *Appl. Opt.*, vol. 57, no. 28, Oct. 1, 2018, Art. no. 8258, doi: [10.1364/AO.57.008258](https://doi.org/10.1364/AO.57.008258).
- [17] B. Rahmani, D. Loterie, G. Konstantinou, D. Psaltis, and C. Moser, "Multimode optical fiber transmission with a deep learning network," *Light Sci. Appl.*, vol. 7, no. 1, 2018, doi: [10.1038/s41377-018-0074-1](https://doi.org/10.1038/s41377-018-0074-1).
- [18] P. Fan, T. Zhao, and L. Su, "Deep learning the high variability and randomness inside multimode fibers," *Opt. Exp.*, vol. 27, no. 15, Jul. 22, 2019, Art. no. 20241, doi: [10.1364/OE.27.020241](https://doi.org/10.1364/OE.27.020241).
- [19] Y. Liu, G. D. Li, Q. Qin, Z. W. Tan, M. G. Wang, and F. P. Yan, "Bending recognition based on the analysis of fiber specklegrams using deep learning," *Opt. Laser Technol.*, vol. 131, Nov. 2020, Art. no. 106424, doi: [10.1016/j.optlastec.2020.106424](https://doi.org/10.1016/j.optlastec.2020.106424).
- [20] A. R. Cuevas, M. Fontana, L. Rodriguez-Cobo, M. Lomer, and J. M. Lopez-Higuera, "Machine learning for turning optical fiber specklegram sensor into a spatially-resolved sensing system. Proof of concept," *J. Lightw. Technol.*, vol. 36, no. 17, pp. 3733–3738, Sep. 1, 2018, doi: [10.1109/JLT.2018.2850801](https://doi.org/10.1109/JLT.2018.2850801).
- [21] K. Simonyan and A. Zisserman, "Very deep convolutional networks for large-scale image recognition," in *Proc. Int. Conf. Learn. Representat.*, 2015, pp. 1–14. [Online]. Available: <https://arxiv.org/abs/1409.1556>
- [22] K. S. C. Kuang, W. J. Cantwell, and P. J. Scully, "An evaluation of a novel plastic optical fibre sensor for axial strain and bend measurement," *Meas. Sci. Technol.*, vol. 13, pp. 1523–1534, 2002, doi: [10.1088/0957-0233/13/10/303](https://doi.org/10.1088/0957-0233/13/10/303).
- [23] H. Di, "Sensing principle of fiber-optic curvature sensor," *Opt. Laser Technol.*, vol. 62, pp. 44–48, 2014, doi: [10.1016/j.optlastec.2014.02.009](https://doi.org/10.1016/j.optlastec.2014.02.009).
- [24] M. Kovacevic, D. Nikezic, and A. Djordjevich, "Monte Carlo simulation of curvature gauges by ray tracing," *Meas. Sci. Technol.*, vol. 15, pp. 1756–1761, 2004.
- [25] K. C. Kao and G. A. Hockham, "Dielectric-fibre surface waveguides for optical frequencies," *Proc. Inst. Elect. Engineers*, vol. 113, no. 7, pp. 1151–1158, Jul. 1966, doi: [10.1049/piee.1966.0189](https://doi.org/10.1049/piee.1966.0189).